Original Article

Harmine loaded Au@MSNs@PEG@Asp6 nano-composites for treatment of spinal metastasis from lung adenocarcinoma by targeting ANXA9 *in vivo* experiment

Houlei Wang[1,2#], Fancheng Chen[1#], Annan Hu[1#], Haifeng Liang[1], Yun Liang[1], Nagashree Seetharamu[3], Huiren Wang[1], Jian Dong[1]

[1]Department of Orthopedic Surgery, Zhongshan Hospital, Fudan University, Shanghai, China; [2]Department of Orthopedic Surgery, Baoshan District Wusong Central Hospital, Fudan University, Shanghai, China; [3]Division of Medical Oncology and Hematology, Northwell Health Cancer Institute, New York, NY, USA

Contributions: (I) Conception and design: Houlei Wang, F Chen; (II) Administrative support: Huiren Wang, J Dong; (III) Provision of study materials or patients: Houlei Wang, H Liang; (IV) Collection and assembly of data: Houlei Wang, A Hu; (V) Data analysis and interpretation: Houlei Wang, Y Liang; (VI) Manuscript writing: All authors; (VII) Final approval of manuscript: All authors.

[#]These authors contributed equally to this work.

Correspondence to: Huiren Wang, PhD; Jian Dong, MD, PhD. Department of Orthopedic Surgery, Zhongshan Hospital, Fudan University, 180 Fenglin Road, Shanghai 200032, China. Email: wang.huiren@zs-hospital.sh.cn; dong.jian@zs-hospital.sh.cn.

Background: Annexin A9 (ANXA9) has been proved to be concerned with cancer development. However, to explore the clinical consequences of ANXA9 in lung adenocarcinoma (LUAD), especially its correlation to spinal metastasis (SM) has no in-depth study. The study was expected to elucidate the mechanism of ANXA9 in regulating SM of LUAD and create a productive nano-composites delivery system targeting this gene for treatment of SM.

Methods: Harmine (HM), a β-carboline extracted from the traditional Chinese herb Peganum harmala, loaded Au@MSNs@PEG@Asp6 (NPS) nano-composites were synthesized. Bioinformatics analysis and clinical specimens' tests were used to verify the association between ANXA9 and prognosis of LUAD with SM. The immunohistochemistry (IHC) was employed to detect the expression levels of the ANXA9 protein in LUAD tissues with or without SM, and its significance in clinic was also explored. ANXA9-siRNA was applied to investigate the molecular mechanism of ANXA9 in tumor behaviors. The HM release kinetics was detected by high performance liquid chromatography (HPLC) method. The cellular uptake efficiency of nanoparticles by A549 cells was observed by fluorescence microscope. Antitumor effects of nanoparticles were assessed in the nude mouse model of SM.

Results: The genomic amplification of ANXA9 was prevalent in LUAD tissues and closely associated with poor outcome and SM ($P<0.01$). The experimental result manifested that high expression of ANXA9 could lead to wretched prognosis and ANXA9 was an independent risk factor for survival ($P<0.05$). After impeding expression of ANXA9, the proliferation and metastatic ability of tumor cells obviously decreased, and expression of matrix metallopeptidase 2 (MMP-2) and matrix metallopeptidase 9 (MMP-9) were considerably downregulated, while the expression of associated oncogene pathway were downregulated ($P<0.01$) as well. The synthesized HM-loaded NPS nano-composites could target to cancer and response to reactive oxygen species (ROS) to release HM slowly. Notably, in comparison to free HM, the nano-composites showed excellent targeting and anti-tumor effects in the A549 cell-bearing mouse model.

Conclusions: ANXA9 may serve as a novel biomarker for predicting poor prognosis in LUAD, and we provided an efficient and targeting drug delivery nano-composites system for precise treatment of SM from LUAD.

Keywords: Nanoparticle; harmine (HM); Annexin A9 (ANXA9); lung adenocarcinoma (LUAD); spinal metastasis (SM)

Submitted Jun 22, 2022. Accepted for publication May 16, 2023. Published online May 26, 2023.
doi: 10.21037/tlcr-23-191
View this article at: https://dx.doi.org/10.21037/tlcr-23-191

Introduction

Lung cancer is one of the most common malignant tumors worldwide and the leading cause of cancer death in China (1). Lung adenocarcinoma (LUAD) in a form of non-small cell lung cancer (NSCLC), accounting for approximately 40–55% of lung cancer incidence (2). With the development of new targeting medicines and treatment strategies, the therapeutic effect of LUAD treatment has been improved greatly (3). However, bone metastasis occurs in 30–40% of lung cancer cases with a majority affecting the spine (4). Despite major advances in LUAD treatment, patients who develop SM have poor prognosis and quality of life (5). In addition to disabling pain, spinal metastasis (SM) can result in a series of events, including paraplegia, quadriplegia and lifelong urinary and fecal incontinence (6). Current treatment of SM including surgery, external beam radiation, brachytherapy and systemic treatment, all of which typically result in temporary, suboptimal benefit (7,8). Thus, comprehensive understanding of the molecular mechanism related to SM from LUAD is urgently needed to enable better interventions to combat this devastating disease.

Annexins (ANXs) are a large family of multifunctional Ca^{2+}-binding proteins with 12 identified family members, including A, B, C, D, and E subgroups that can bind to anionic biomolecules (9). The members of the ANX family have diverse biological functions that are mainly involved in the secretion and transportation of vesicles, mitosis, cell senescence and apoptosis, calcium ion channel signaling, and cell growth (10). In particular, specific subgroups of membrane coupling protein A (ANXA) are closely related to cancers (11,12). For example, increased expression of ANXA9, a family member of ANXA, has been associated with gastric cancer (13), head and neck squamous cell carcinomas (14), and colorectal cancer (15). Some researchers also found that ANXA9 expression was associated with immune-related biological function. ANXA9 expression was also correlated with the infiltration level of $CD8^+$ T cells, neutrophils, and dendritic cells in tumor (16). Function enrichment analyses revealed that immune network plays an important role in LUAD progression by interacting with its related genes (17). However, the exact connection between ANXA9 and LUAD remains unclear.

Harmine (HM), a β-carboline extracted from the traditional Chinese herb *Peganum harmala*, has a wide range of pharmacological effects on ion channels, muscle, the cardiovascular system, and the central nervous system (18). Recent studies have demonstrated that HM has the ability to inhibit tumor cells (e.g., NSCLC) (19,20). However, poor absorption and bioavailability of HM when administered systemically has resulted in inability to realize its therapeutic potential (21). In addition, due to neurotropic nature of HM, serious toxicity to the central nervous system is also an important factor impeding its clinical application (18). Using a precise drug delivery system to specific areas of disease might mitigate some of these challenges and provide an effective strategy to deliver this anti-tumor agent effectively and safely.

Among the available delivery systems, mesoporous silica-Au nano-composites have been extensively studied because of their high drug loading efficiency, good biocompatibility, easy fabrication and modification, and Au-dependent photothermal therapy ability (22,23). For example, a recently published study reported successful employment of nanotheranostic system for pH triggered-multimodal cancer therapy (24).

Highlight box

Key findings

- Report here about key findings of the study.
- We present a novel therapeutic strategy of HM@NPS nano-composites to target SM of LUAD.

What is known and what is new?

- The serious toxicity of traditional Chinese medicine HM impeded its clinical application.
- We provide a highly efficient drug delivery system for potential precise treatment of SM from LUAD.

What is the implication, and what should change now?

- Report here about implications and actions needed.
- The study aimed to evaluate the prognostic value of ANXA9 in LUAD patients and its relationship with the development of SM and provided the targeted therapeutic strategy and multidisciplinary collaboration is needed for the treatment of SM.

In this study, we aimed to investigate the relationship between ANXA9 and prognosis of LUAD patients, with a particular focus on cell migration, invasion and development of SM. Parallelly, through several experiments involving cell lines and animal models, we assessed the ability of HM to inhibit ANXA9 and its associated pathways. We evaluated sensitivity and targetability of HM to LUAD and SM from LUAD. We designed smart HM-loaded Au@MSNs@PEG@Asp6 (HM@NPS) nano-composites to target LUAD cells and release HM in response to reactive oxygen species (ROS). We herein present the results of our study evaluating the prognostic value of ANXA9 in LUAD patients and its relationship with development of SM. We also present the results of our experiments showing the therapeutic ability of HM@NPS nano-composites to target SM of LUAD in the nude mouse model of SM. We present this article in accordance with the ARRIVE reporting checklist (available at https://tlcr.amegroups.com/article/view/10.21037/tlcr-23-191/rc).

Methods

Chemicals

Sodium borohydride (NaBH4), 1-ethyl-3-(3-dimethly-aminopropyl) carbodiimide (EDC), tetraethyl orthosilicate (TEOS), ascorbic acid, sodium hydroxide, concentrated sulfuric acid, hydrochloric acid (12 mol/L), ethanol, (3-aminopropyl) triethoxysilane (APTES), cetyltrimethyl ammonium bromide (CTAB), N-hydroxysuccinimide (NHS), and tetrachloroauric acid ($HAuCl_4 \cdot 3H_2O$) were bought from Sigma-Aldrich (St. Louis, MO, USA). We purchased HM from ChemeGen (Los Angeles, CA, USA); Asp6 was purchased from Shanghai Botai Biotechnology Co., Ltd. (Shanghai, China).

Bioinformatics analysis

Based on The Cancer Genome Atlas (TCGA) dataset for LUAD, gene expression and DNA copy-number variation (CNV) of 526 tumor tissues and 59 normal lung tissues were analyzed (http://www.cbioportal.org/). The one-sided Jonckheere-Terpstra test was applied to assess the effect of ANXA9 CNV on expression. The gene set enrichment analysis (GSEA) algorithm was used to identify the pathways of significant enrichment between high and low expression of ANXA9. The study was conducted in accordance with the Declaration of Helsinki (as revised in 2013).

DNA CNV detection

The DNA of specimens of LUAD tissues and paired normal lung tissues were obtained by Tguide S32 Magnetic Tissue Genomic DNA Kit (TIANGEN Biotech. Co. Ltd., Beijing, China). The ANXA9 CNV was detected by QX200 Droplet Digital PCR Assay (Bio-Rad, Hercules, CA, USA).

Immunohistochemistry

Immunohistochemical (IHC) staining of the ANXA9 protein from LUAD and SM specimens was carried out according to the standard protocol using anti-ANXA9 (ab235891; Abcam, Cambridge, MA, USA) and the corresponding secondary antibody. The IHC assessment was performed by two independent pathologists. The results were scored from 0 to 3 and specimens were divided into 2 groups according to their score: the IHC score of low expression group was less than 50% and that of high expression was over 50%.

Cell transfection

Human lung cancer cell lines (A549) and human lung bronchial epithelial 16HBE cells (Chinese Academy of Sciences, Shanghai, China) were routinely cultured in Dulbecco's modified Eagle medium (DMEM) with 10% fetal bovine serum (FBS) and 1% penicillin/streptomycin.

The coding sequence of ANXA9 was cloned into pLVX-Puro plasmids (Clontech, Mountain View, CA, USA) to elevate ANXA9 expression, and RNA interference sequence of ANXA9 was cloned into linearized pLKO.1 plasmids (Addgene, Watertown, MA, USA) to down-regulate ANXA9 expression. The interference sites and corresponding primer sequences were as follows: ANXA9 (shRNA-1, position 302–320, 5'-CCCTCAGGACCTTCTTGAA-3'; shRNA-2, position 461–479, 5'-CCCAACAGGACCTGATGAA-3'; shRNA-3, position 832–850, 5'-GGACCTAGCAGAGAGGAAA-3'). Recombinant plasmids together with the packaging plasmids psPAX2 and pMD2G were co-transfected into 293T cells. After 48 hours, recombined vectors were enriched for transducing cells. The negative control was cells with pLKO.1-scramble short hairpin (sh)RNA or

blank pLVX-Puro transduction.

Synthesis of HM@NPS nano-composites

Synthesis of Au@mesoporous silica nanoparticles

The synthesis of Au@mesoporous silica nanoparticles (Au@MSNs) was performed according to a previous study, with minor modifications (25). Briefly, a 9.4 mL aqueous solution containing 0.75 mmoL CTAB and 2.5×10^{-3} mmoL $HAuCl_4$ was mixed with 0.6 mL ice-cold NaBH4 aqueous solution (0.01 M) and CTAB-capped Au seeds were obtained immediately. Then, the growth of seeds was carried out in a mixture solution at 30 ℃, containing 5 mmoL CTAB, 0.025 mmoL $HAuCl_4$, 0.5 mmoL H_2SO_4, and 0.01 mmoL ascorbic acid. Following that, the reactive system was centrifuged, washed 3 times, and diluted to 20 mL with water. Whilst stirring, 200 μL of 0.1 M NaOH aqueous solution was supplemented. After that, 60 μL of 20% TEOS methanol solution was injected under gentle stirring, and repeated every 30 minutes for a total of 3 times. The mixture was stored at 26–28 ℃ for 3 days. Then, the sample was obtained by centrifugation and washed 3 times with ethanol. The sample was then dried at 60 ℃ oven for 24 hours to remove ethanol. Then, 100 μL HCl was added to the 100 mL ethanol solution with 0.5 g Au@MSN and the reactive systems were stirred for 8 hours at 60 ℃ to remove CTAB from the as-prepared sample. The products were enriched by centrifugation and dried in a 60 ℃ oven. The products in this stage were denoted as Au@MSNs.

Preparation of amine-functionalized Au@MSNs

The amine-functionalized Au@MSNs were obtained by treatment with APTES. The detailed steps were as follows: 100 mg Au@MSNs was dispersed in 200 mL ethanol, and it was refluxed at 78 ℃ for 12 hours. Then, 0.5 mL APTES was added. After centrifugation at 10,000 rpm for 5 minutes, the precipitate was washed with water and ethanol. Finally, the obtained Au@MSNs-NH2 was dried at 60 ℃ for further use.

The HM loading on amine-functionalized Au@MSNs

Amine-functionalized Au@MSNs (100 mg) were incubated with 10.0 mL of 25 mg/mL HM for 24 hours and collected by centrifugation at 10,000 rpm for 20 minutes. The products were freeze-dried and named as HM@Au@MSNs.

PEG grafting onto the surface of HM@Au@MSNs

Firstly, 0.192 g EDC and 0.115 g NHS were solved into 100 mL of water (pH 6.0) and simultaneously the reactive system was vigorously stirred for 30 minutes. Secondly, 50 mg HM@Au@MSNs in 10 mL deionized water were supplemented and the mixture was stirred for 6 hours. Thirdly, the obtained conjugate was washed with deionized water and dried using vacuum freeze dryer. The final obtained products were named as HM@Au@MSNs@PEG.

Asp6 grafting onto the surface of HM@Au@MSNs@PEG

A total of 10 mg HM@Au@MSNs@PEG was dispersed into 100 mL water (pH 6.0). Then, 0.192 g EDC and 0.115 g NHS aqueous solution were added and stirred for 30 minutes. Afterwards, 10 mL of 0.5/mL ASP6 aqueous water was added and stirred for 6 hours. The product, named as HM@Au@MSNs@PEG@Asp6 (HM@NPS) nanocomposites, was obtained by centrifugation and dried using a vacuum freeze dryer.

Characterization of assays

Physical and chemical structure analysis

The morphologies were observed by a transmission electron microscope (TEM; JEM-2100F, JEOL Ltd., Tokyo, Japan). Fourier transform infrared (FTIR) spectroscopy were recorded by a Nicolet iS10 instrument (Thermo Fisher, Waltham, MA, USA). Thermogravimetry analysis was recorded by a STA449C thermal analysis instrument (Netzsch, Selb, Germany). High performance liquid chromatography (HPLC) was measured by Waters Alliance HPLC system (Waters, Milford, MA, USA).

HM release in response of ROS

To study the role of ROS in HM release from HM@NPS nano-composites, drug release experiments were carried out at 37 ℃ in phosphate-buffered solutions (PBS; pH 7.4) with different concentrations of H_2O_2 ranging from 0 to 1 mM. The content of free HM in the incubation solution was measured at given time intervals by HPLC method.

Photothermal analysis

The photothermal conversion efficiency of HM@NPS nano-composites at different time points was measured at 808 nm by semiconductor laser device (GCSLS-05-007; Daheng New Epoch Technology, Inc., Beijing, China). The power density was set at 1 W cm^{-2}; PMCS (5 mg/mL) was irradiated by near infrared (NIR) laser light transfer. A PT-3S thermo-detector (Optex Co., Ltd., Tokyo, Japan) was

used to detect the temperature change.

Cell Counting Kit-8 (CCK-8) assay

Cell proliferation was assessed by CCK-8 assay. Cells with 3×10^3 cells/well concentration were seeded and routinely cultured in 96-well plates for 12 hours. The A549 and 16HBE cells were treated with HM (0.5, 1, 2, 4, and 8 μg/mL). After 24 or 48 hours, the CCK-8 reagent was added for another 1 hour of cell culture. The absorbance of each well was determined at 450 nm.

Cellular uptake

The uptake ability of A549 cells to NPS nano-composites was assessed by confocal laser scanning microscopy. Briefly, A549 cells with 3×10^4 cells/well concentration in a 24-well plate were exposed to 2 μg/mL NPS nano-composites. After 6 hours of incubation, the sections of cell nucleus, cytoskeleton, and NPS nano-composites were treated with 4',6-diamidino-2-phenylindole (DAPI; Beyotime Biotechnology, Shanghai, China), fluorescein isothiocyanate (FITC)-phalloidin (Abcam), and Cy7 (MedChemExpress) for 40 minutes in sequence, which were determined by confocal laser scanning microscopy with 405, 562, and 488 nm of excitation wavenumber, respectively. For TEM detection, the samples were treated according to a recently described procedure after fixation with 4% glutaraldehyde.

Transwell assay

The A549 cells (3×10^4 cells/well) were cultured in the 6-well plate at 37 ℃ overnight. The cell migration and invasion were measured according to a previous study (26). After fixed and stained with crystal violet, tumor cell migration and invasion were analyzed under a microscope.

Quantitative real-time polymerase chain reaction (qRT-PCR)

Total RNA was extracted by Trizol reagent (Invitrogen, Carlsbad, CA, USA) according to the experimental protocol, and reverse transcribed into cDNA with RevertAid First Strand cDNA Synthesis Kit (Thermo Fisher, USA). qRT-PCR was conducted using SYBR green PCR Master Mix (Thermo Fisher, USA) on an ABI7300 system. The primers were as follows: ANXA9 (5'-GGCAGCTCATCTCACGAAAC-3' and 5'-CAGCAGAGCCATCACAATCC-3'); glyceraldehyde 3-phosphate dehydrogenase (GAPDH) (5'-AATCCCATCACCATCTTC-3' and 5'-AGGCTGTTGTCATACTTC-3'). The relative abundance of genes was quantified by using the comparative $2^{-\Delta\Delta Ct}$ with GAPDH as an internal control.

Western blot

The proteins of interest were separated by sodium dodecyl sulfate-polyacrylamide gel electrophoresis (SDS-PAGE), and transferred onto a nitrocellulose membrane. Membranes were further blocked with 5% skim milk, and immersed into antibodies solution against ANXA9 (ab166621), MMP-2 (ab97779), MMP-9 (ab73734; all from Abcam), AKT (#9272), p-AKT (#9271), and GAPDH (#5174; all from Cell Signaling Technology, USA]. Then, the membranes were immersed into the secondary antibody solution linked to horseradish peroxidase (HRP; Beyotime, Shanghai, China). Signals were captured by a chemiluminescence system.

Precise targeting of HM@NPS nano-composites against spinal metastasis from lung adenocarcinoma using mouse model (LUAD SM)

A total of 40 4–6-week-old BALB/c nude mice (half male/half female) were obtained from the Jiesijie Laboratory Animal Co., Ltd. (Shanghai, China). Experiments were performed under a project license (No. ZS2019-032) granted by the Institutional Animal Ethics Committee of Zhongshan Hospital, in compliance with institutional guidelines for the care and use of animals. A protocol was prepared before the study without registration. The mice were randomly divided into four groups (n=10), which were group control, group HM, group NPS and group HM@NPS.

First, 200 μL of 1×10^6 A549 cells were injected into the left ventricle to establish spinal metastases mice models. A549 is a LUAD cell line derived from a patient with the highest tendency to form spine metastases using previously described methods (27). After successful creation of the LUAD SM model *in vivo*, the mice were then divided into four groups, with each group consisting of 10 mice. After 3 weeks, in one group of mice (Group A), HM@NPS nano-composites were injected into the tail vein at a concentration of 0.25 mg/mouse/day for 4 weeks. The HM@NPS nano-composites fluorescent images were obtained through In

Vivo Imaging System (IVIS) 200 system (PerkinElmer, Waltham, MA, USA) at 0, 6, 12, and 24 hours to verify the bio-distribution of HM@NPS nano-composites. Both HM and NPS nanocomposites were chosen as controls (Groups B and C). Group D mice were not treated with anything. The surviving A549 cells *in vivo* were detected via bioluminescence at 0, 2, and 4 weeks in each group of mice. The lesions were also assessed using micro-computed tomography (CT). The mice were sacrificed intravenous injection at the end of the experiment. Heart, liver, lung, spleen, kidneys, and SM were collected, washed, fixed with 4% paraformaldehyde, and displayed by paraffin sections for toxicity evaluation after hematoxylin and eosin (H&E) staining.

Statistical analysis

Statistical analysis was conducted by GraphPad Prism 8.0.2 (GraphPad Software Inc., La Jolla, CA, USA). Data from independent triplicates were displayed as mean ± standard deviation. After test of normality of continuous variables, analysis of variance (ANOVA) and Student's *t*-test were used to analyze the differences among groups. The Kaplan-Meier method and Cox's proportional hazards regression model were used to calculate overall survival and the log-rank test was used for comparisons. All tests were two-sided, and significant effects were defined when $P<0.05$.

Results

Evaluation on the prognosis predictor role of ANXA9 in LUAD

As a form of structural genomic variation, CNV is ubiquitous in human beings and is closely related to disease susceptibility or resistance to cancer treatment. *Figure 1A-1D* shows the prevalence of ANXA family CNV in LUAD using the TCGA database. It can be seen that the *ANXA6*, *ANXA9*, and *ANXA13* genes show amplification in LUAD patients, and ANXA9 had the most significant gains (*Figure 1A*). High expression of *ANXA9* was associated with a poor prognosis in LUAD patients (*Figure 1B*). Additionally, in comparison with the non CNV group, the ANXA9 messenger RNA (mRNA) level in the ANXA9-gained CNV group was significant higher (*Figure 1C*). Differential expression analysis indicated that ANXA9 mRNA level is increased in LUAD tissues compared with normal tissues (*Figure 1D*). In paired tissue specimens, (*Figure 1E-1N*), the ANXA9 mRNA level was significantly higher in tumor tissue compared with normal tissue in LUAD patients (*Figure 1E*). We analyzed the ANXA9 CNV by RT-PCR in clinical specimens to verify its consistency with bioinformatics data. The RT-PCR revealed that ANXA9 amplification was detected in 4 of 32 (12.5%) samples in cohort 1 and 12 of the 97 (12.4%) samples in cohort 2 (*Figure 1F*). The LUAD cases with ANXA9 amplification exhibited close associations with poorer prognosis than those without alteration in both groups (*Figure 1G,1H*). Our analysis also suggested that high expression of ANXA9 and shortening of survival time in LUAD patients were driven by its copy-number alterations.

The ANXA9 protein expression pattern was observed by IHC analysis in our experiment (*Figure 1I,1J*). Kaplan-Meier analysis showed that high expression of ANXA9 was associated with a poor prognosis in this cohort of 97 LUAD patients (*Figure 1K*). Multivariate regression analysis including pertinent clinical and pathological features indicated that the ANXA9 protein expression is an independent predictor of LUAD aggressiveness with significant HR for predicting clinical outcomes (*Figure 1L*). Specific to LUAD with SM (n=59), high expression of ANXA9 was associated with a poor prognosis as shown in *Figure 1M,1N*. These data indicate that ANXA9 might be an independent prognosis predictor and play an important role in regulating spinal metastases from LUAD.

Investigation on the inhibition effect of ANXA9 and possible molecular mechanism on the migration and invasion of A549 cells

To verify whether ANXA9 indeed plays an oncogenic role in LUAD progression *in vivo*, we performed GSEA. The results showed that the ANXA9 expression was associated with metastasis and the AKT signaling pathway (*Figure 2A*). The designed shRNAs could specifically target ANXA9 and efficiently down-regulate the expression of ANXA9 in A549 cells (*Figure 2B,2C*). The migration and invasion ability of A549 cells were measured before or after changing the expression level of ANXA9. As shown in *Figure 2D-2F*, knockdown of ANXA9 decreased the migration and invasion of A549 cells. Knockdown of ANXA9 also resulted in decreased MMP-3 and MMP-9 protein and p-AKT levels (*Figure 2G*).

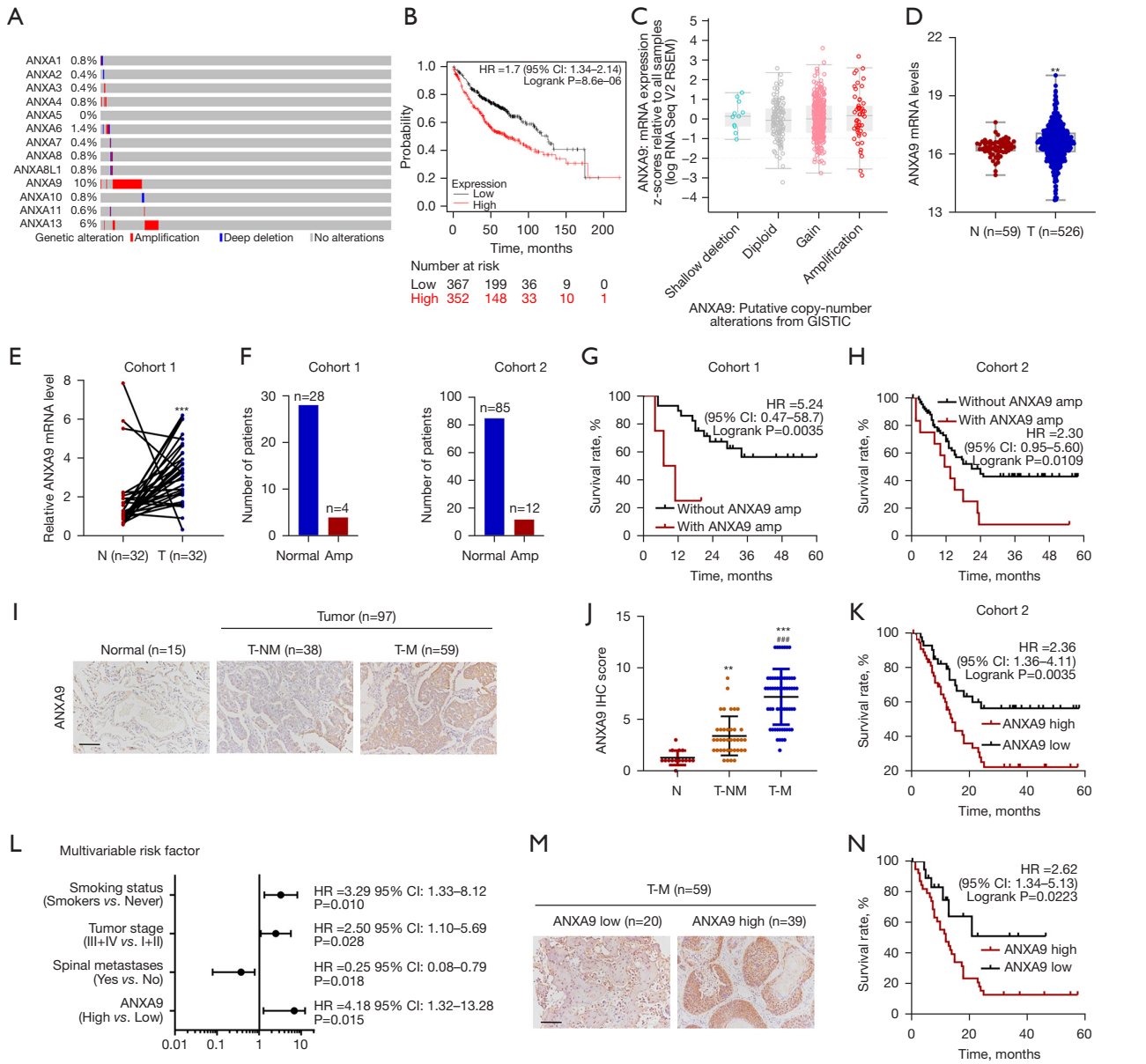

Figure 1 ANXA9 genomic amplification was prevalent in LUAD tissues and associated with poor outcome and spinal metastases. (A) Representative CNV analysis of ANXA family genes up-regulated in LUAD tissues from TCGA database. (B) Survival rate of LUAD patients from TCGA database. (C) In TCGA database, ANXA9 mRNA level with ANXA9-gained CNV samples were significantly increased by comparison with the samples without CNV (1-sided Jonckheere-Terpstra test, P<0.01). (D) ANXA9 expression in LUAD tissues (n=526) and normal liver tissues (n=59) from TCGA dataset. (E) The expression of ANXA9 in LUAD tissues and paired normal lung tissues (n=32) from cohort 1 was measured by qRT-PCR. (F) qRT-PCR analysis on ANXA9 copy number in 2 cohorts. (G,H) Survival analysis of clinical specimens with or without ANXA9 amplification in 2 cohorts. (I,J) The expression of ANXA9 in LUAD tissues with or without SM and normal lung tissues from cohort 2 was measured by IHC. Scale bars: 100 μm. (K) Survival analysis of clinical specimens with high or low ANXA9 expression in cohort 2. (L) Multivariate regression analysis of cohort 2. (M) The expression of ANXA9 in spinal tissues of patients with spinal metastasis from cohort 2 was measured by IHC. Scale bars: 100 μm. (N) Survival analysis was performed between patients with spinal metastasis and with high or low ANXA9 expression from cohort 2. **, P<0.01, ***, P<0.001 compared with N. ###, P<0.001 compared with T-NM. CI, confidence interval; HR, hazard ratio; IHC, immunohistochemistry; LUAD, lung adenocarcinoma; CNV, copy-number variation; TCGA, The Cancer Genome Atlas; qRT-PCR, quantitative real-time polymerase chain reaction; mRNA, messenger RNA; SM, spinal metastasis.

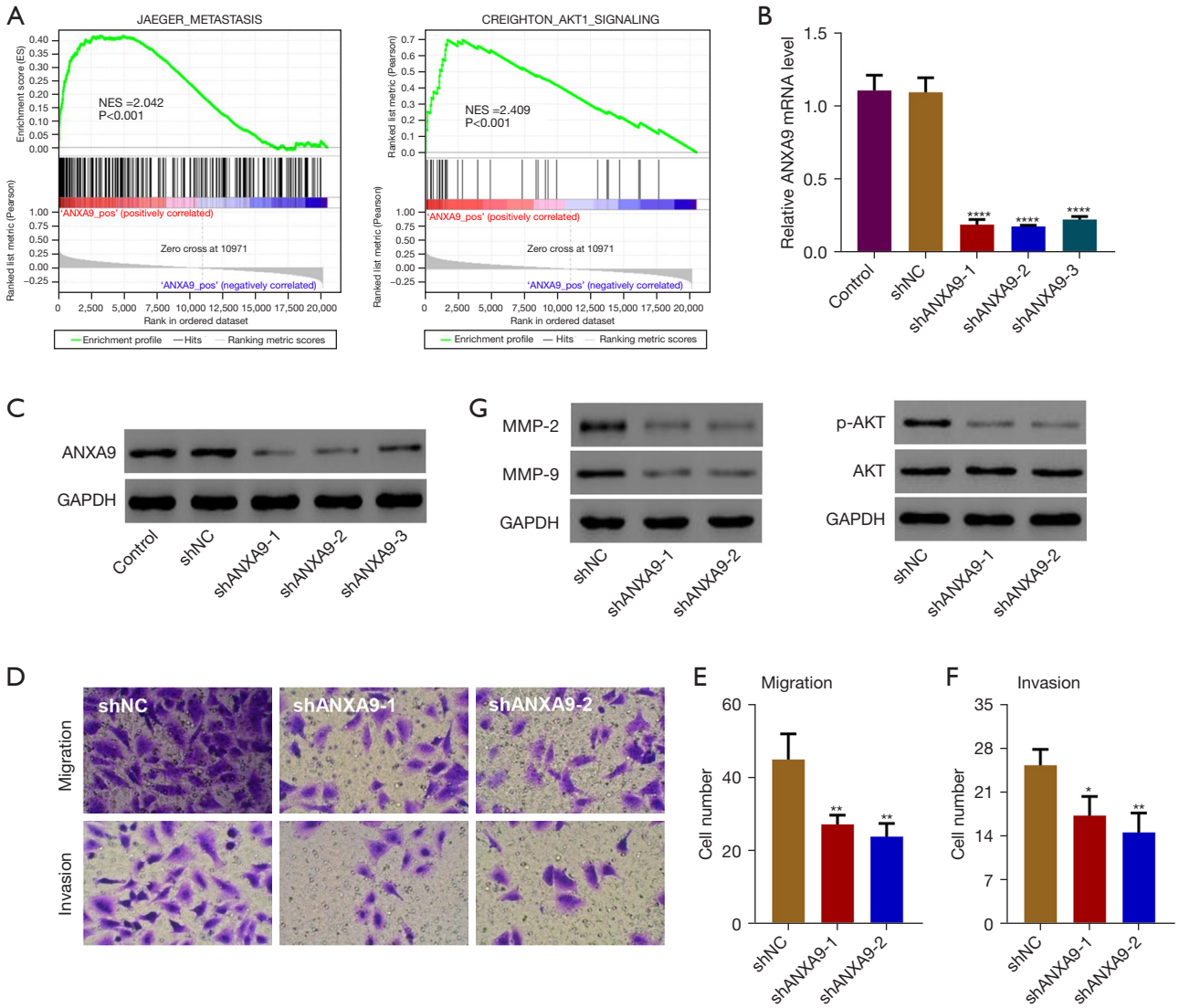

Figure 2 ANXA9 knockdown inhibited cell migration and invasion in A549 cells. (A) GSEA demonstrated ANXA9 expression was associated with the metastasis and AKT signaling pathway. (B) mRNA level of ANXA9, (C) ANXA9 expression in A549 cells transduced with indicated plasmids. (D-F) Cell migration and invasion was analyzed by Transwell assay via crystal violet staining (×200). (G) expression of MMP-2, MMP-9, p-AKT, and AKT in A549 cells transduced with indicated plasmids. *, P<0.05; **, P<0.01; ****, P<0.0001 compared with shNC. GSEA, gene set enrichment analysis; mRNA, messenger RNA; NC, negative control; NES, normalized enrichment score.

Design and synthesis of a smart HM@NPS nano-composites for ROS-sensitive HM release

The Au@MSNs nanoparticles were obtained by a sol-gel method. *Figure 3A* shows the TEM image of Au@MSNs. The diameter of Au@MSNs particles ranged from 80 to 100 nm and Au@MSNs nanoparticles had a core-shell structure. The silica shell with about 20 nm thickness was composed of disordered mesopores and the gold core with about 60 nm diameter showed a dense structure. This gold core-silica shell structure was specifically designed to supply mesoporous space for drugs and simultaneously act as a photothermal agent.

We employed FTIR analysis to monitor the evolvement of the preparation HM@NPS nano-composites. As shown in *Figure 3B*, free silanol stretching vibration mode at 960 cm^{-1} weakened when the PEG was successfully grafted on the surface of the Au@MSNs. The comparative strong C=O

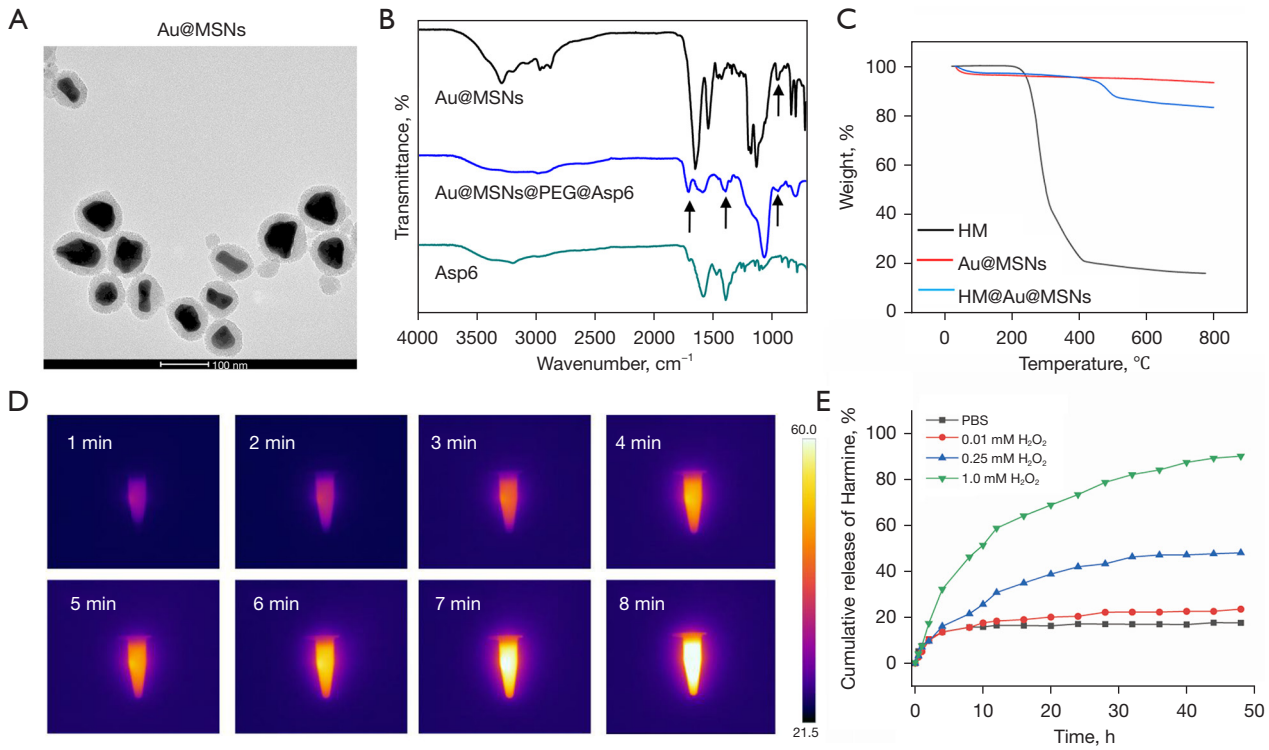

Figure 3 Characterization of HM@NPS nano-composites. (A) TEM image of Au@MSNs. (B) FTIR image of Asp6, Au@MSNs, and HM@NPS nano-composites, respectively. The arrows further indicate the successful synthesis of HM@NPS. (C) Thermogravimetry analysis of isotherms of HM, Au@MSNs and HM@NPS nano-composites. (D) Aqueous dispersion of HM@NPS nano-composites (5 mg/mL) at different time points under laser irradiation (808 nm) with 1.0 W/cm^2 condition. (E) The drug release profiles of HM@NPS nano-composites incubated with different concentrations of H_2O_2. MSN, mesoporous silica nanoparticles; PEG, polyethylene glycol; HM, harmine; NPS, nanoparticles; PBS, phosphate-buffered solution; TEM, transmission electron microscope; FTIR, Fourier transform infrared spectroscopy.

absorption peak at 1,700 cm^{-1} and C-N stretching vibration peak at 1,400 cm^{-1} indicated that the Asp6 molecules had been successfully introduced to the nanoparticles. *Figure 3C* shows the weight loss of HM, Au@MSNs, and HM@NPS nano-composites with the increase of temperature by thermogravimetry analysis. The Au@MSNs were relatively stable but the weight of HM@NPS nano-composites gradually reduced and the weight loss rate reached about 10% from 200 to 500 ℃, corresponding to the burning of HM. Therefore, the loading efficiency of HM on NPS nano-composites could be calculated to be 100 mg/g. Compared with water, the temperature of the aqueous dispersion of Au@MSNs dramatically increased to 60 ℃ within 8 min after irradiation (*Figure 3D*), indicating the good photothermal conversion capacity of HM@Au@MSNs.

TK linkers (from H2N-PEG-TK-COOH) are sensitive to ROS and the fracture of TK linkers has been shown to cause the release of HM from pores of HM@NPS nano-composites (28). To investigate the HM release kinetics from HM@NPS nanocomposites in response to ROS, we utilized H_2O_2 as typical ROS stimuli in *in-vitro* experiments, and the release profiles of the encapsulated HM from HM@NPS nano-composites under different H_2O_2 concentration were monitored by HPLC. As shown in *Figure 3E*, without H_2O_2, less than 20% of HM could leak out from HM@NPS nanocomposites in 50 hours due to the protection of PEG, proving the effectiveness of anchoring the nano-valves by the TK linkers. In contrast, H_2O_2 significantly promoted the release of HM from HM@NPS nano-composites and the HM release rate positively correlated with the concentration of H_2O_2. The highest cumulative release of HM in 50 hours reached over 80% when the concentration of H_2O_2 was 1 mM. This suggested that the HM release was H_2O_2-sensitive owing to the ROS-cleavable TK linkers.

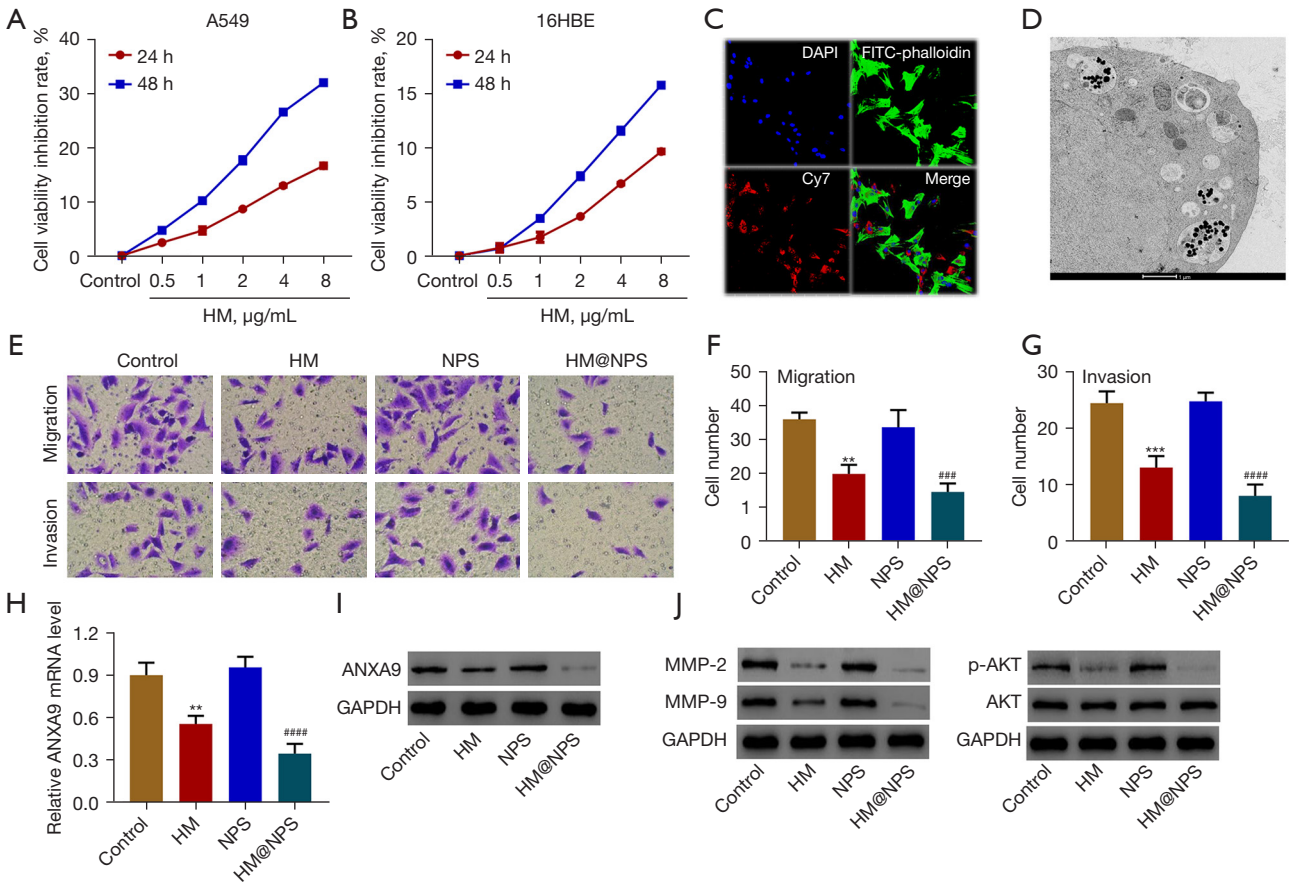

Figure 4 Effects of HM@NPS nano-composites on A549 cells behaviors. Cell viability of (A) A549 and (B) 16HBE cells incubated with different concentrations of HM for 24 and 48 h. (C) Confocal laser scanning microscope images (blue: nuclei stained with DAPI, red: HM@NPS nano-composites stained with Cy7, green: cytoskeleton stained with FITC-phalloidin, ×40). (D) TEM images indicated the intracellular distribution of HM@NPS nano-composites in A549 cells. (E-G) Cell migration and invasion, as determined by Transwell assays via crystal violet staining (×200). (H-J) expression of ANXA9, MMP-2, MMP-9, p-AKT, and AKT of A549 cells incubated with HM, NPS or HM@NPS nano-composites. **, P<0.01; ***, P<0.001 compared with control. ###, P<0.001; ####, P<0.0001 compared with NPS nano-composites. HM, harmine; NPS, nanoparticles; DAPI, 4',6-diamidino-2-phenylindole; FITC, fluorescein isothiocyanate; TEM, transmission electron microscope; FTIR, Fourier transform infrared spectroscopy.

Effect of HM, NPS, and HM@NPS nano-composites on cell behaviors

The cytotoxicity of NPS nano-composites and HM was assessed using human lung normal cells (16HBE) and lung cancer cells (A549). As for NPS nano-composites, over 90% of A549 and 16HBE cells after exposure to NPS nano-composites for 24 hours and 48 hours survived even at a concentration of 2 μg/mL, indicating good biological safety (data not shown). As for free HM (*Figure 4A*,*4B*), the CCK-8 assay results revealed that A549 cancer cells are more sensitive to HM than 16HBE normal cells, and the inhibition rate of HM on A549 was about twice that of 16HBE cells; both positively correlated with HM concentration. Less than 70% of A549 cells survived after exposure to 8 μg/mL of HM for 48 hours (*Figure 4A*), and for 16HBE cells, the survival rate was about 85% (*Figure 4B*). These data indicated that HM might be toxic to tumor cells but can absolve normal cells.

To investigate the cellular uptake of NPS nano-composites, A549 cells were exposed to NPS nano-composites and observed by confocal laser microscopy (cells with 6 h of exposure to NPS nano-composites) and TEM (cells with 4 h of exposure to NPS nano-composites). Both

could easily capture the NPS nano-composites into the cells. The NPS nano-composites mainly locate at cytoplasm (*Figure 4C*) and exist in vesicles (*Figure 4D*).

The migration and invasion of A549 cells were compared after exposure to HM, NPS, and HM@NPS nano-composites. In comparison with the untreated control, the NPS nano-composites had no effect on the migration and invasion of A549 cells (*Figure 4E-4G*). However, the treatment with free HM or HM@NPS nano-composites significantly attenuated the migration and invasion of A549 cells, with the effect of HM@NPS nano-composites being stronger than that of free HM (*Figure 4E-4G*). These results demonstrate that the loading of HM on NPS nano-composites can enhance the effect of HM against A549 cells.

Figure 4H,4I show the ANXA9 mRNA and protein levels in A549 cells after exposure to HM, NPS, or HM@NPS nano-composites by RT-PCR and Western blot analysis, respectively. It can be seen that the NPS nano-composites had no effect on ANXA9 mRNA level. Contrarily, HM@NPS nano-composites exhibited much stronger inhibition effect than HM on the ANXA9 gene transcription and protein expression. Simultaneously, the decrease of several key proteins' expression (e.g., MMP-3, MMP-9, p-AKT) was also detected in A549 cells after exposure to HM or HM@NPS nano-composites (*Figure 4J*).

The ANXA9-overexpression A549 cells model was established to confirm the role of ANXA9 in tumor progression. The RT-PCR results demonstrated the successful transfection of ANXA9 expression in A549 cells, characterized with a higher level of ANXA9 mRNA level (*Figure 5A*). By comparison with A549 cells without ANXA9 transfection, the ANXA9 overexpression cells significantly increased the migration and invasion, and simultaneously induced high protein expression (e.g., MMP-3, MMP-9, p-AKT) (*Figure 5B-5E*). Importantly, HM@NPS nano-composites or HM could reverse these effects and the reversion of HM@NPS nano-composites was stronger than that of HM (*Figure 5B-5E*).

Investigation on the targeting and therapeutic effects of HM@NPS nano-composites against SM lung cancer mice model

To verify the targeting effect of HM@NPS nano-composites, the SM lung cancer model was established by left ventricle injection of A549 cells. After 3 weeks, the HM@NPS nano-composites were intravenously injected. *Figure 6A* shows the bioluminescence of A549 cells and fluorescence (red) signal of HM@NPS nano-composites at the indicated times. It clearly demonstrates that HM@NPS nano-composites could target to A549 cells after intravenous injection at 12 hours. The H&E staining in *Figure 6B* demonstrates no significant pathological changes in liver, spleen, kidney, heart, and lung tissue samples from all the groups. HM however, inhibited the survival and SM of A549 cells in mice (*Figure 6C,6D*). Importantly, the inhibitory effects of HM in A549 cells-bearing mice were enhanced by HM@NPS nano-composites (*Figure 6C,6D*). Overall, consistent with our *in vitro* findings, our *in vivo* experiment showed that HM@NPS nano-composites effectively target LUAD SM with negligible systemic toxicity.

Discussion

ANXA9 is a novel prognostic marker for gastric cancer patients, that has been shown to regulate cell differentiation, invasion, and migration (13); however, the underlying molecular mechanisms of ANXA9 in SM of LUAD has remained unknown. In this study, we present for the first time, through bioinformatics analysis of TCGA database and assays using clinical specimens, the correlation between LUAD and ANXA9. We also show possible mechanisms by which ANXA9 promotes SM of cancer cells. Similarly to previous studies demonstrating the increased expression of ANXA9 in other cancers (14,15), we also found an increased level of ANXA9 with CNVs in LUAD tissues. This suggests that amplification of the *ANXA9* gene is the basis of ANXA9 overexpression in LUAD.

We also verified that metastasis and AKT signaling pathway-related genes were enriched in LUAD tissues with higher expression of ANXA9. In line with our bioinformatics findings, ANXA9 knockdown inhibited, and its overexpression promoted, the invasion and migration of A549 cells. This is consistent with previous observations concerning ANXA9 (13) and other ANXA proteins in different cancers, including lung cancer (29,30). Specifically, it has been well documented that ANXA3 regulates epithelial mesenchymal transition (EMT) and lymph node metastasis in pancreatic cancer through the PI3K/AKT signaling pathway (31) and ANXA11 promotes invasion, migration, and EMT progress in hepatocellular carcinoma via the activation of AKT signaling (32). However, molecular mechanisms by which ANXA9 regulates AKT signaling activation in SM of LUAD has not

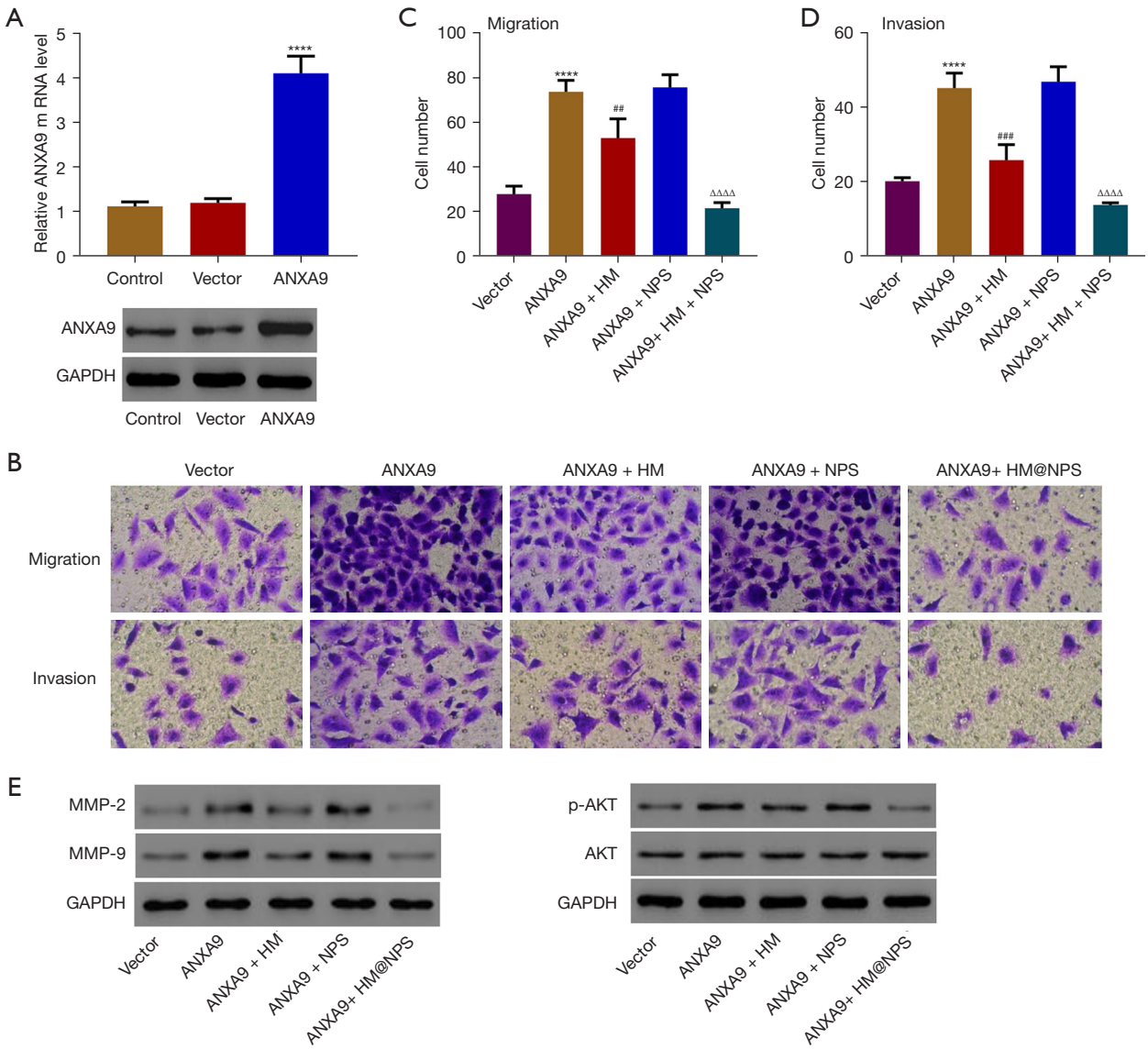

Figure 5 ANXA9 overexpression increases cell migration and invasion in A549 cells and HM@NPS nano-composites exhibited stronger inhibition effect on A549 cells with ANXA9 overexpression than free HM. (A) mRNA and protein expression of ANXA9 in A549 cells transduced with indicated plasmids. (B-D) Cell migration and invasion, as determined by Transwell assays via crystal violet staining (×200). (E) expression of MMP-2, MMP-9, p-AKT, and AKT in A549 cells transduced with indicated plasmids and incubated with HM, NPS, or HM@NPS nano-composites, respectively. ****, P<0.0001 compared with vector. ##, P<0.01; ###, P<0.001 compared with ANXA9. ΔΔΔΔ, P<0.0001 compared with ANXA9 + NPS. HM, harmine; NPS, nanoparticles; mRNA, messenger RNA.

been previously reported. Our study provides a glimpse of possible mechanisms involved in this specific condition.

In addition to insufficient understanding on of its molecular mechanisms involved in its pathogenesis in LUAD, SM presents a unique challenge from a therapeutic perspective. Despite major advances in LUAD treatment, effective SM management remains an unmet need and SM is often associated with poor survival and quality of life. Recently, nano-delivery system-based cancer therapy has been shown to be a promising treatment strategy for SM patients, with minimal systemic side effects, maximum tumoricidal effect, and absence of multi-drug resistance.

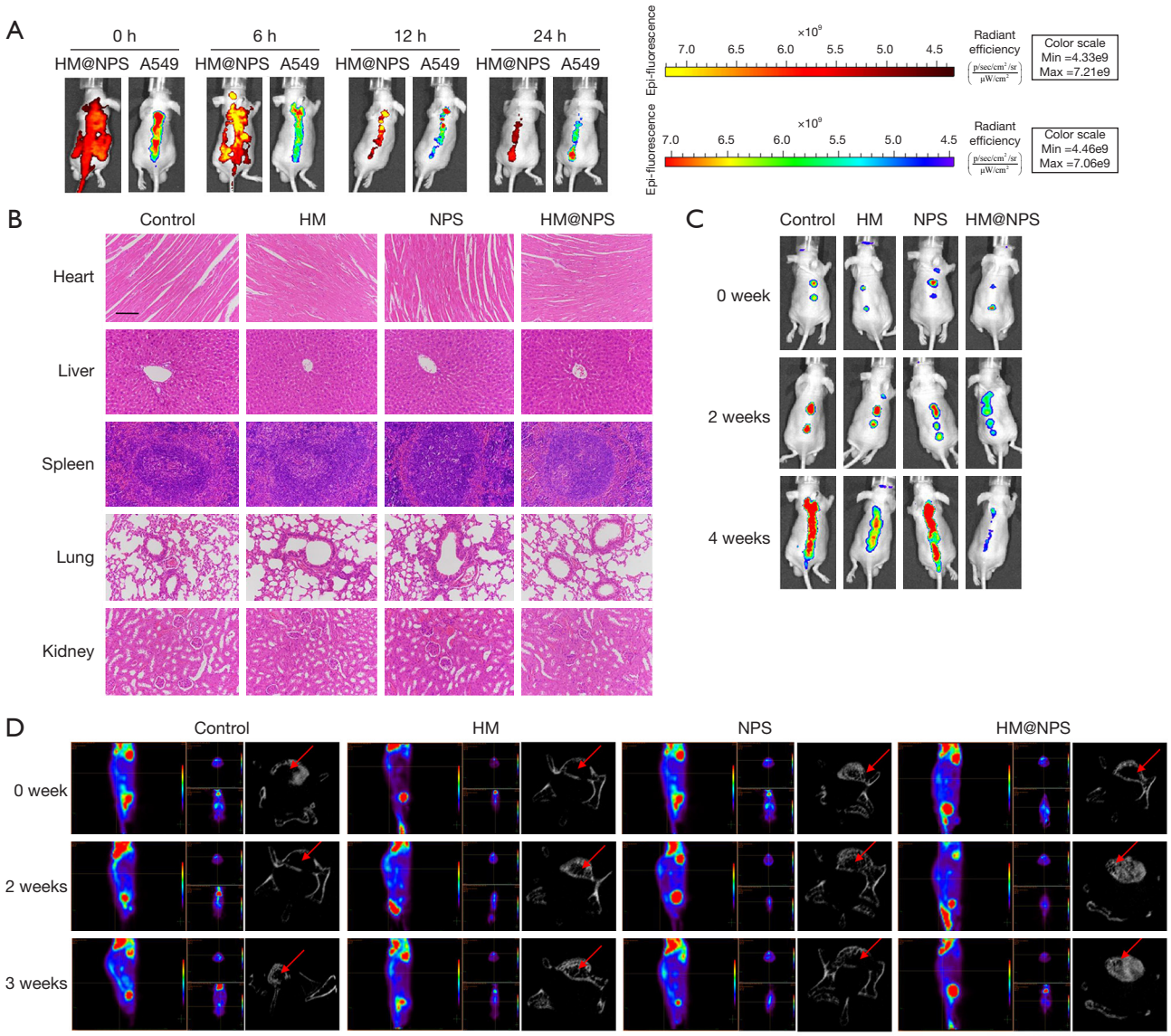

Figure 6 Anti-tumor and anti-metastasis efficacies of HM@NPS nano-composites in lung cancer model mice bearing A549 cells. (A) Representative fluorescence (HM@NPS nano-composites) and bioluminescence (A549 cells) images in the spinal metastatic model at 0, 6, 12, and 24 h after intravenous injection of HM@NPS nano-composites (0.25 mg/mouse/d). (B) Images of H&E-stained sections obtained from the major organs (heart, liver, spleen, lung, and kidney) of mice 4 weeks post injection with HM (0.25 mg/mouse/d), NPS (0.25 mg/mouse/d) or HM@NPS nano-composites (0.25 mg/mouse/d). Scale bars: 100 μm. (C) A549 cell survival in the mice monitored with an IVIS 200 system. (D) Micro-CT images of local destruction (arrows) in the affected spine of the tumorigenic mice. HM, harmine; NPS, nanoparticles; H&E, hematoxylin and eosin; IVIS, In Vivo Imaging System; micro-CT, micro-computed tomography.

Here, we successfully designed and synthesized smart HM@NPS nanocomposites for targeted treatment of SM from LUAD. Firstly, the high surface area and large pore volume of our construct supported high loading efficiency of HM (100 mg/g). Secondly, the link of Asp6, a bio-inspired oligopeptide present in osteopontin, allowed the HM@NPS nano-composites to specifically target to lung cancer SM cells. Thirdly, the TK linker (from H2N-PEG-TK-COOH) allowed release of HM preferentially in response to ROS thus protecting the molecule and allowing for its slow release. In this study, we chose HM, a Chinese herb extract as the loaded drug against SM of LUAD due to

its outstanding anti-tumor activity (20,33). Studies have shown that HM has pro-apoptotic, anti-proliferation, anti-invasion, anti-migration, and anti-metastasis functions in NSCLC (34) and other malignancies (33,35). In this study, we not only show effective tumor inhibition with SM but also shed additional insight into its mechanism of action by clearly demonstrating the inhibitory effect of HM on AKT signaling pathway. Our findings suggest that HM may be a candidate drug for precise treatment of LUAD SM. Considering the positive correlation between the ANXA9 expression and metastasis as well as AKT signaling pathway, and the observation that ANXA9 expression can be induced by HM in LUAD cells, we hypothesized that ANXA9 may be an effective target for HM (36,37). Encouraged by the *in-vitro* anti-tumor cells effects of HM@NPS nano-composites, *in vivo* antitumor efficacy of HM@NPS nano-composites was evaluated in the lung cancer SM mice model. Excitingly, HM@NPS nano-composites exhibited the ability to target A549 cells in 12 hours. At 4 weeks after injection of A549 cells in mice, tumors in the HM@NPS nano-composites treatment group almost ceased to progress by comparison with other groups suggesting outstanding anti-tumor efficacy. The use of nano-composites system allowed achievement comparable efficacy and increasing of biological activity of a drug compared to traditional chemotherapy. At the same time, such formulations significantly increase the drug load and may increase its bioavailability, response to ROS, reduce side effects, and, as a consequence, improve drug efficacy. It may provide novel treatment strategies for some lung adenocarcinoma with spinal metastasis.

Conclusions

In conclusion, ANXA9 expression correlates with cell migration and invasion of A549 cells via the AKT signaling pathway in LUAD in general, and specifically in LUAD SM. HM inhibits this but free HM is associated with significant systemic toxicity. HM@NPS nano-composites fabricated by coating PEG, ASP6, and HM onto Au@MSN nanoparticles can precisely target lung cancer SM cells, through its ability to release HM in response to ROS. The HM@NPS nano-composites has low cytotoxicity to normal tissues and exhibits a good biological safety. Importantly, HM@NPS nanocomposites can effectively reduce LUAD cancer cell migration and invasion compared to free HM in. This study sheds light on a novel mechanism potentially involved in SM of LUAD and a novel strategy to treat this challenging disease. This study also reinforces that understanding of the mechanisms of action of natural products derived from traditional Chinese herbs can facilitate the development of safe and effective anticancer drugs.

Acknowledgments

The authors appreciate the academic support from AME Lung Cancer Collaborative Group.
Funding: This work was funded by the Shanghai Sailing Program (No. 21YF1433100) and Shanghai Pujiang Program (No. 22PJD010).

Footnote

Reporting Checklist: The authors have completed the ARRIVE reporting checklist. Available at https://tlcr.amegroups.com/article/view/10.21037/tlcr-23-191/rc

Data Sharing Statement: Available at https://tlcr.amegroups.com/article/view/10.21037/tlcr-23-191/dss

Peer Review File: Available at https://tlcr.amegroups.com/article/view/10.21037/tlcr-23-191/prf

Conflicts of Interest: All authors have completed the ICMJE uniform disclosure form (available at https://tlcr.amegroups.com/article/view/10.21037/tlcr-23-191/coif). The authors have no conflicts of interest to declare.

Ethical Statement: The authors are accountable for all aspects of the work, including ensuring that any questions related to the accuracy or integrity of any part of the work have been appropriately investigated and resolved. The study was conducted in accordance with the Declaration of Helsinki (as revised in 2013). Experiments were performed under a project license (No. ZS2019-032) granted by the Institutional Animal Ethics Committee of Zhongshan Hospital, in compliance with institutional guidelines for the care and use of animals.

References

1. Xia C, Dong X, Li H, et al. Cancer statistics in China and United States, 2022: profiles, trends, and determinants. Chin Med J (Engl) 2022;135:584-90.
2. Hutchinson BD, Shroff GS, Truong MT, et al. Spectrum of Lung Adenocarcinoma. Semin Ultrasound CT MR 2019;40:255-64.
3. Succony L, Rassl DM, Barker AP, et al. Adenocarcinoma spectrum lesions of the lung: Detection, pathology and treatment strategies. Cancer Treat Rev 2021;99:102237.
4. Huang X, Shi X, Huang D, et al. Mutational characteristics of bone metastasis of lung cancer. Ann Palliat Med 2021;10:8818-26.
5. Liu C, Yi J, Jia J. Diagnostic and prognostic nomograms for bone metastasis in small cell lung cancer. J Int Med Res 2021;49:3000605211050735.
6. Candido PBM, Peria FM, Pinheiro RP, et al. Outcomes and survival of spinal metastasis with epidural compression. J Craniovertebr Junction Spine 2021;12:287-93.
7. Wong YC, Chau WWJ, Kwok KO, et al. Incidence and Risk Factors for Implant Failure in Spinal Metastasis Surgery. Asian Spine J 2020;14:878-85.
8. Osborn VW, Lee A, Yamada Y. Stereotactic Body Radiation Therapy for Spinal Malignancies. Technol Cancer Res Treat 2018;17:1533033818802304.
9. Méndez-Barbero N, Gutiérrez-Muñoz C, Blázquez-Serra R, et al. Annexins: Involvement in cholesterol homeostasis, inflammatory response and atherosclerosis. Clin Investig Arterioscler 2021;33:206-16.
10. Li YZ, Wang YY, Huang L, et al. Annexin A protein family in atherosclerosis. Clin Chim Acta 2022;531:406-17.
11. Wu W, Jia G, Chen L, et al. Analysis of the Expression and Prognostic Value of Annexin Family Proteins in Bladder Cancer. Front Genet 2021;12:731625.
12. Vecchi L, Araújo TG, Azevedo F, et al. Phospholipase A(2) Drives Tumorigenesis and Cancer Aggressiveness through Its Interaction with Annexin A1. Cells 2021;10.
13. Zhou Y, Qiu C, Wang T, et al. High Expression of Annexin A9 Promotes Cell Proliferation and Migration in Gastric Cancer via the TGF-β Signaling Pathway. J Environ Pathol Toxicol Oncol 2021;40:87-94.
14. Salom C, Álvarez-Teijeiro S, Fernández MP, et al. Frequent Alteration of Annexin A9 and A10 in HPV-Negative Head and Neck Squamous Cell Carcinomas: Correlation with the Histopathological Differentiation Grade. J Clin Med 2019;8.
15. Yu S, Bian H, Gao X, et al. Annexin A9 promotes invasion and metastasis of colorectal cancer and predicts poor prognosis. Int J Mol Med 2018;41:2185-92.
16. Liu L, Xu S, Huang L, et al. Systemic immune microenvironment and regulatory network analysis in patients with lung adenocarcinoma. Transl Cancer Res 2021;10:2859-72.
17. Zhang T, Yu S, Zhao S. ANXA9 as a novel prognostic biomarker associated with immune infiltrates in gastric cancer. PeerJ 2021;9:e12605.
18. Li Z, Chen L, He C, et al. Improving anti-tumor outcomes for colorectal cancer therapy through in situ thermosensitive gel loading harmine. Am J Transl Res 2020;12:1658-71.
19. Li Y, Zhou D, Xu S, et al. DYRK1A suppression restrains Mcl-1 expression and sensitizes NSCLC cells to Bcl-2 inhibitors. Cancer Biol Med 2020;17:387-400.
20. Le Moigne R, Subra F, Karam M, et al. The β-Carboline Harmine Induces Actin Dynamic Remodeling and Abrogates the Malignant Phenotype in Tumorigenic Cells. Cells 2020;9.
21. Jiang J, Ma T, Zhang L, et al. The transdermal performance, pharmacokinetics, and anti-inflammatory pharmacodynamics evaluation of harmine-loaded ethosomes. Drug Dev Ind Pharm 2020;46:101-8.
22. Zeng S, Liu S, Lan Y, et al. Combined Photothermotherapy and Chemotherapy of Oral Squamous Cell Carcinoma Guided by Multifunctional Nanomaterials Enhanced Photoacoustic Tomography. Int J Nanomedicine 2021;16:7373-90.
23. Duan Q, Yang M, Zhang B, et al. Gold nanoclusters modified mesoporous silica coated gold nanorods: Enhanced photothermal properties and fluorescence imaging. J Photochem Photobiol B 2021;215:112111.
24. Esmaeili Y, Khavani M, Bigham A, et al. Mesoporous silica@chitosan@gold nanoparticles as "on/off" optical biosensor and pH-sensitive theranostic platform against cancer. Int J Biol Macromol 2022;202:241-55.
25. Zhang Z, Wang L, Wang J, et al. Mesoporous silica-coated gold nanorods as a light-mediated multifunctional theranostic platform for cancer treatment. Adv Mater 2012;24:1418-23.
26. Zhang M, Yang X, Chen S, et al. GPR12 inhibits migration and promotes apoptosis in esophageal cancer and hypopharyngeal cancer cells. Thorac Cancer 2021;12:1525-35.

27. Liu P, Wang H, Liang Y, et al. LINC00852 Promotes Lung Adenocarcinoma Spinal Metastasis by Targeting S100A9. J Cancer 2018;9:4139-49.
28. Hu JJ, Lei Q, Peng MY, et al. A positive feedback strategy for enhanced chemotherapy based on ROS-triggered self-accelerating drug release nanosystem. Biomaterials 2017;128:136-46.
29. Elakad O, Li Y, Gieser N, et al. Role of Annexin A1 in Squamous Cell Lung Cancer Progression. Dis Markers 2021;2021:5520832.
30. Chuang MC, Lung JH, Chen YC, et al. The Association of Annexin A1 and Chemosensitivity to Osimertinib in Lung Cancer Cells. Cancers (Basel) 2021;13.
31. Wan X, Guo D, Zhu Q, et al. microRNA-382 suppresses the progression of pancreatic cancer through the PI3K/Akt signaling pathway by inhibition of Anxa3. Am J Physiol Gastrointest Liver Physiol 2020;319:G309-g22.
32. Liu Z, Wang Y, Wang L, et al. Long non-coding RNA AGAP2-AS1, functioning as a competitive endogenous RNA, upregulates ANXA11 expression by sponging miR-16-5p and promotes proliferation and metastasis in hepatocellular carcinoma. J Exp Clin Cancer Res 2020;319:G309-22.
33. Tan B, Li Y, Zhao Q, et al. The impact of Harmine hydrochloride on growth, apoptosis and migration, invasion of gastric cancer cells. Pathol Res Pract 2020;216:152995.
34. Shen J, Wang B, Zhang T, et al. Suppression of Non-Small Cell Lung Cancer Growth and Metastasis by a Novel Small Molecular Activator of RECK. Cell Physiol Biochem 2018;45:1807-17.
35. Nafie E, Lolarga J, Lam B, et al. Harmine inhibits breast cancer cell migration and invasion by inducing the degradation of Twist1. PLoS One 2021;16:e0247652.
36. Zhu YG, Lv YX, Guo CY, et al. Harmine inhibits the proliferation and migration of glioblastoma cells via the FAK/AKT pathway. Life Sci 2021;270:119112.
37. Ock CW, Kim GD. Harmine Hydrochloride Mediates the Induction of G2/M Cell Cycle Arrest in Breast Cancer Cells by Regulating the MAPKs and AKT/FOXO3a Signaling Pathways. Molecules 2021;26.

(English Language Editor: J. Jones)

Cite this article as: Wang H, Chen F, Hu A, Liang H, Liang Y, Seetharamu N, Wang H, Dong J. Harmine loaded Au@MSNs@PEG@Asp6 nano-composites for treatment of spinal metastasis from lung adenocarcinoma by targeting ANXA9 *in vivo* experiment. Transl Lung Cancer Res 2023;12(5):1062-1077. doi: 10.21037/tlcr-23-191